Cavity Quantum Optomechanical Nonlinearities and Position Measurement beyond the Breakdown of the Linearized Approximation

J. Clarke,[1,*] P. Neveu,[2] K. E. Khosla,[1] E. Verhagen,[2] and M. R. Vanner[1,†]
[1]QOLS, Blackett Laboratory, Imperial College London, London SW7 2BW, United Kingdom
[2]Center for Nanophotonics, AMOLF, Science Park 104, 1098 XG Amsterdam, The Netherlands

(Received 22 July 2022; revised 5 May 2023; accepted 28 June 2023; published 3 August 2023)

Several optomechanics experiments are now entering the highly sought nonlinear regime where optomechanical interactions are large even for low light levels. Within this regime, new quantum phenomena and improved performance may be achieved; however, a corresponding theoretical formalism of cavity quantum optomechanics that captures the nonlinearities of both the radiation-pressure interaction and the cavity response is needed to unlock these capabilities. Here, we develop such a nonlinear cavity quantum optomechanical framework, which we then utilize to propose how position measurement can be performed beyond the breakdown of the linearized approximation. Our proposal utilizes optical general-dyne detection, ranging from single to dual homodyne, to obtain mechanical position information imprinted onto both the optical amplitude and phase quadratures and enables both pulsed and continuous modes of operation. These cavity optomechanical nonlinearities are now being confronted in a growing number of experiments, and our framework will allow a range of advances to be made in, e.g., quantum metrology, explorations of the standard quantum limit, and quantum measurement and control.

DOI: 10.1103/PhysRevLett.131.053601

Introduction.—Cavity quantum optomechanics utilizes the cavity-enhanced radiation-pressure interaction to enable precision control of mechanical degrees of freedom. Significant progress has been made in the linearized regime where, for large coherent drives, mechanical displacements give rise to small optical phase shifts. However, there is significant current experimental drive to increase single-photon coupling rates, which necessarily gives rise to the nonlinear response of the cavity and the breakdown of the linearized approximation. Importantly, such behavior occurs well before the strong single-photon-coupling regime where qualitatively different phenomena may be explored [1–3]. Crucially, due to the nonlinearities of radiation pressure and the cavity response, mechanical displacements give rise to significant rotations to the optical field in phase space, and thus the mechanical signal is transduced onto both the phase and amplitude quadratures. This radiation-pressure nonlinearity allows for selective position-squared measurements [4], the generation of macroscopic superposition states [5–7], non-Gaussian entanglement [8–11], and even optomechanical photon blockade for strong single-photon coupling [12,13]. Recent experimental progress has seen rapid improvements in coupling rates, with cold-atom implementations reaching the strong single-photon coupling regime [14,15] and, notably even well within the weak single-photon coupling regime, optical rotations have now been observed, which cannot be described by the linearized approximation [16–18].

Closely connected to the radiation-pressure interaction, optomechanical position measurement is a critical component for many research areas ranging from mechanical quantum state engineering to tests of fundamental physics. Prominent example position-measurement applications include ultrasensitive accelerometry [19,20], yoctogram-resolution mass sensing [21], zeptonewton weak-force sensing [22], single-spin detection [23], and even biomedical sensing [24]. The precision enabled by cavity optomechanical position measurement also provides a valuable tool for fundamental physics experiments such as gravitational wave detection [25] and searches for new physics [26] including dark matter [27] and non-Newtonian gravity [28].

Owing to the interplay between radiation-pressure backaction and optical quantum noise, optomechanical position measurement is a rich field of study. Prominently, this interplay leads to the standard quantum limit (SQL) [29], which describes restrictions on position measurement sensitivity and is now well understood experimentally [30–32]. Furthermore, within the SQL, weak continuous position measurement [33] combined with feedback [34,35] can be utilized to cool mechanical oscillators toward their ground state [36,37]. To go beyond the SQL, backaction-evading (BAE) measurements, such as two-tone drive [38–41] or pulses much shorter than the

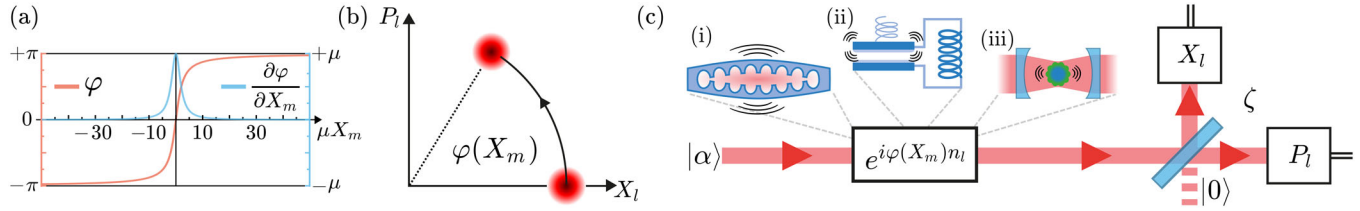

FIG. 1. Cavity quantum optomechanical nonlinearities. (a) Plot of the optical phase $\varphi(X_m)$ and the dimensionless mechanical momentum kick per photon $\partial\varphi(X_m)/\partial X_m$ arising from the cavity-enhanced nonlinear optomechanical interaction. Here, $\mu \propto g_0/\kappa$ is the dimensionless coupling strength, X_m is the mechanical position quadrature, and the detuning is $\Delta = 0$. (b) In optical phase space there is a position-dependent rotation of an input coherent state owing to the nonlinearities of the radiation-pressure interaction and the cavity response. Our framework goes well beyond both the linearized regime, which approximates the rotation as a displacement, and treatments where the interaction is modeled as the unitary $e^{i\mu n_l X_m}$, which neglects the cavity response. (c) Position measurement scheme. An optical coherent state $|\alpha\rangle$ interacts with an optomechanical cavity and is then measured by general-dyne detection, which may be realized with a beam splitter of variable transmission coefficient ζ, vacuum on one input, and amplitude and phase homodyne measurements at the outputs. Our scheme and theoretical formalism are broadly applicable with example nonlinear optomechanical systems including (i) photonic crystals, (ii) microwave LC resonators, and (iii) levitation-based or cold-atom implementations.

mechanical period [42–45], may be employed. Thus far, the aforementioned position-measurement techniques operate in the linearized regime, but advances in coupling rates are now forcing experiments to confront the cavity optomechanical nonlinearities.

In this Letter, we develop a framework of optomechanics that accounts for the nonlinearities of both the radiation-pressure interaction and the cavity response. Secondly, we utilize this framework to propose how both pulsed and continuous position measurement can be performed in the nonlinear regime. To measure the mechanical signal transduced onto the optical field, we employ the established technique of general-dyne detection [46–48], which ranges from single to dual homodyne. Our formalism allows the optomechanical interaction to be described throughout the entire cavity phase response and enables new regimes of operation, such as the stochastic Gaussian regime we identify and term here. Our framework will enable a broad range of further studies and applications including the important tools of position measurement, squeezing by measurement, and mechanical state tomography to be performed beyond the linearized approximation.

Nonlinear position-measurement scheme.—Radiation pressure is described by the cubic Hamiltonian $H/\hbar = -g_0 a^\dagger a(b + b^\dagger)$, where g_0 is the optomechanical coupling rate, and a (b) is the annihilation operator of the cavity field (mechanical mode). In addition to this nonlinearity, the full response of the cavity itself is also nonlinear; i.e., the optical phase shift depends nonlinearly on the mechanical position and asymptotes to $\pm\pi$ for large displacements. The combination of these nonlinearities is captured by the Heisenberg-Langevin and input-output equations, which yields the relation $a_{\rm out} = f(X_m)a_{\rm in}$, where $a_{\rm in}$ and $a_{\rm out}$ are the optical input and output fields and $f(X_m) = \{1 + i[(\mu/2)X_m + (\Delta/\kappa)]\}/\{1 - i[(\mu/2)X_m + (\Delta/\kappa)]\}$ is the nonlinear response function. Here, X_m (P_m) is the dimensionless mechanical position (momentum) quadrature, $\mu = \sqrt{8}g_0/\kappa$ is the nonlinear coupling strength, κ is the cavity amplitude decay rate, which is dominated by external coupling, and Δ is the detuning from the cavity's resonance at zero mechanical displacement. In Fig. 1(a), we plot the optical phase $\varphi(X_m) = \arg(f)$ and the dimensionless mechanical momentum kick per photon $\partial\varphi(X_m)/\partial X_m$ to help visualize these nonlinearities. We then obtain the nonlinear optomechanical unitary $U = e^{i\varphi(X_m)n_l}$, where n_l is the photon number operator of the field entering or leaving the cavity. Notably, for this model, the only approximation made here is that the cavity is adiabatic, i.e., $\dot{a} \simeq 0$ [49]. Thus, our framework is applicable beyond the linearized regime and, furthermore, overcomes the limitations of previous works that model the optomechanical interaction as $e^{i\mu n_l X_m}$, e.g., Refs. [50,51], by accounting for the nonlinear response of the cavity. Figure 1(b) shows the rotation of an optical coherent state $|\alpha\rangle$ by angle $\varphi(X_m)$ following the nonlinear optomechanical interaction, where information about the mechanical position is encoded on both the optical phase P_l and amplitude X_l quadratures. The optical field is then measured by general-dyne detection [cf. Fig. 1(c)], which uses two homodyne detectors to measure both optical quadratures in a proportion controlled by a variable beam splitter B with transmission coefficient ζ.

Nonlinear pulsed position measurement.—A pulsed interaction much shorter than a mechanical period enables a BAE position measurement [42,43] as the mechanical free evolution (and, indeed, mechanical dissipation) is negligible during this timescale. Such operations require the unresolved-sideband regime ($\kappa \gg \omega_m$) to accommodate the pulse within the cavity bandwidth. Here, we consider such a pulsed interaction taking into account the cavity optomechanical nonlinearities. Following the nonlinear interaction U, the general-dyne measurement outcomes are then used to estimate the mechanical position. The interaction and measurement are described by the

measurement operator $\Upsilon = \langle X_l|\langle P_l|BU|\alpha\rangle|0\rangle$, which localizes the mechanical state according to $\rho \to \Upsilon\rho\Upsilon^\dagger/\mathcal{P}$, where $\mathcal{P} = \mathrm{tr}(\Upsilon^\dagger\Upsilon\rho)$ is the probability for the general-dyne outcome (X_l, P_l). More explicitly, Υ is

$$\Upsilon = \frac{1}{\sqrt{\pi}}\exp\left[-\frac{1}{2}(X_l - \sqrt{1-\zeta^2}X_\alpha f_R)^2 - \frac{1}{2}(P_l - \zeta X_\alpha f_I)^2 - i\zeta X_\alpha P_l f_R + i\sqrt{1-\zeta^2}X_\alpha X_l f_I - \frac{i}{2}(1-2\zeta^2)X_\alpha^2 f_R f_I\right], \tag{1}$$

where $\alpha = X_\alpha/\sqrt{2}$ is the coherent optical amplitude, assumed to be real without loss of generality, and $f_R = \mathrm{Re}[f(X_m)]$ and $f_I = \mathrm{Im}[f(X_m)]$ [49].

We consider a resonant pulsed drive ($\Delta = 0$) and an initial thermal mechanical state with position variance $\sigma^2 = \langle X_m^2\rangle = \bar{n} + 1/2$ for mean occupation $\bar{n}$. The pulsed interaction gives rise to optical phase shifts depending on the mechanical position distribution and the nonlinearity of $\varphi(X_m)$. Such optical states, with spread determined by $\mu\sigma$, are plotted in Fig. 2(a) using the Husimi-Q function. Note that, with increasing $\mu\sigma$, the maxima of Q move away from $X_l = X_\alpha$ toward $X_l = -X_\alpha$ and the probability of landing within the linear response quickly vanishes. In the limit $\mu\sigma \to \infty$, the input coherent state rotates through an angle $\pm\pi$ in phase space and the mechanical state is unchanged.

Optical loss, including detection inefficiencies, are modeled by a beam splitter of transmission η placed before the general-dyne detector [52]. As the pulsed unitary U is a function of mechanical position X_m alone, optical loss will induce changes in the mechanical momentum [49], while the only effect to the final position marginal is to reduce the strength of the measurement via $X_\alpha \to \eta X_\alpha$ in Eq. (1).

The Bayesian inference associated with the general-dyne measurement reduces the mechanical variance from σ^2 to σ_f^2, which, in contrast to the linearized regime, depends on the measurement outcome (X_l, P_l). As X_l and P_l are continuous variables, we average over all measurement outcomes to quantify the performance of reducing the position variance $\mathbb{E}[\sigma_f^2] = \int dX_l \int dP_l \mathcal{P}(X_l, P_l)\sigma_f^2$ [53]. Figure 2(b) shows the averaged variance $\mathbb{E}[\sigma_f^2]$ as a function of $\mu\sigma$ for the optimal beam splitter transmission coefficient ζ_{opt} demonstrating squeezing well below the ground-state width. Here, ζ_{opt} is computed numerically and is plotted in Fig. 2(c) up to a maximum value of $\mu\sigma$ corresponding to $g_0/\kappa \approx 0.16$ for the fixed $\sigma^2 = 500$. At small and large $\mu\sigma$, the Q function is aligned mostly along the P_l axis, and, hence, the optimal beam splitter transmission coefficient is close to $\zeta = 1$, which agrees with the predictions of the linearized approximation for small $\mu\sigma$. While for intermediate $\mu\sigma$, Q is aligned mostly parallel to the X_l axis, so the optimal setting is closer to $\zeta = 0$. For comparison,

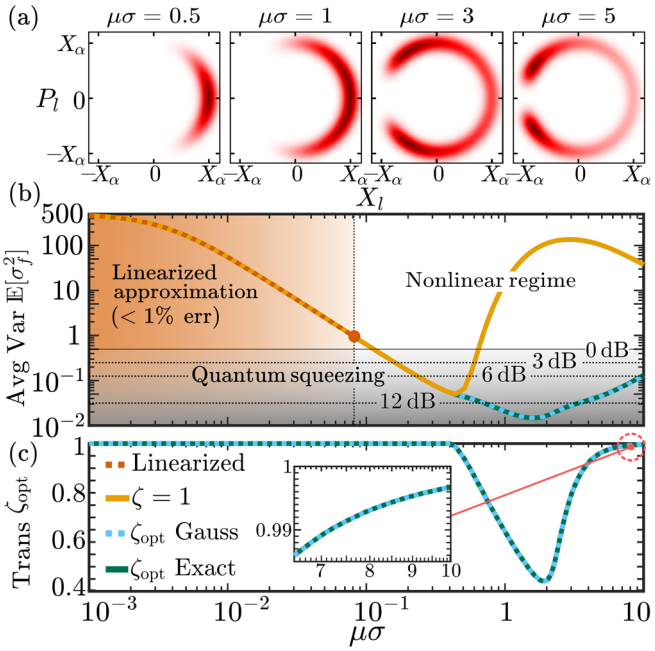

FIG. 2. Nonlinear pulsed position measurement. (a) Q functions of the optical pulse after the optomechanical interaction for $X_\alpha = 10$ and increasing $\mu\sigma$. For an animation, see the Supplemental Material [49]. [Color scale: white to dark red corresponds to $Q = 0$ to $Q = \max(Q)$.] (b) Plot of the mechanical position variance averaged over all measurement outcomes, using either the optimal general-dyne or a phase-homodyne measurement ($\zeta = 1$), as a function of $\mu\sigma$ for $X_\alpha = 200$, and $\sigma^2 = 500$. The gray shaded area indicates quantum squeezing, and for these parameters squeezing below 12 dB is achievable using the optimal general-dyne. The orange shaded area indicates where the error from the linearized approximation is less than 1%, which ends at $\mu\sigma = 0.08$. (c) Plot of the optimal beam splitter transmission coefficient ζ_{opt}. Agreement is seen between the exact case and the Gaussian approximation.

Fig. 2(b) also plots $\mathbb{E}[\sigma_f^2]$ for a phase-homodyne measurement $\zeta = 1$, which misses the mechanical information encoded on the optical amplitude quadrature causing the averaged variance to grow after $\mu\sigma \simeq 0.5$. Thus, despite ζ_{opt} being close to 1 at high $\mu\sigma$, the $\mathbb{E}[\sigma_f^2]$ curves for ζ_{opt} and $\zeta = 1$ still differ and we explore their convergence for even higher values of $\mu\sigma$ in the Supplemental Material [49]. The nonlinear pulsed model we introduce here enables BAE position measurement well beyond the validity of the linearized regime, even when only the phase quadrature is measured. Moreover, Fig. 2(b) shows that the amount of quantum squeezing continues to increase as one exits the linearized regime. A Gaussian approximation in X_m may also be made to the position measurement [49], which agrees with the exact theory for all $\mu\sigma$, and with the linearized approximation within its range of applicability, as shown in Fig. 2.

Nonlinear continuous position measurement.—In addition to pulsed measurements, our scheme in Fig. 1(c) can be

used for continuous position measurement, where the record of general-dyne outcomes can be used to best estimate the quantum trajectory of the mechanical motion in the presence of the nonlinearities via a stochastic master equation (SME). The SME is derived by writing the optical drive as $|\alpha|^2 = 2kdt$, where k describes the photon flux, and expanding Eq. (1) to first order in dt [49]. The full SME, including mechanical open-system dynamics, is

$$d\rho = -\frac{i}{\hbar}[H_0,\rho]dt + \mathcal{D}[c]\rho dt + \mathcal{D}[L]\rho dt + \sqrt{(1-\zeta^2)\eta}\mathcal{H}[c]\rho dW_{X_l} + \zeta\sqrt{\eta}\mathcal{H}[-ic]\rho dW_{P_l}, \quad (2)$$

where $H_0/\hbar = \omega_m b^\dagger b$, ω_m is the mechanical angular frequency, the superoperators are given by $\mathcal{D}[O]\rho = O\rho O^\dagger - \frac{1}{2}\{O^\dagger O,\rho\}$ and $\mathcal{H}[O]\rho = O\rho + \rho O^\dagger - \langle O + O^\dagger\rangle\rho$, the measurement output operator is $c = \sqrt{2k}f(X_m)$, and $L = \sqrt{(4\gamma k_b T)/(\hbar\omega_m)}X_m + i\sqrt{(\hbar\omega_m\gamma)/(4k_bT)}P_m$, which models quantum Brownian motion [54]. Here, T is the environmental temperature, γ is the mechanical decay rate, and η is the measurement efficiency. Further, the Wiener increments for the X_l and P_l measurements obey $dW_i dW_j = \delta_{i,j}dt$ and $\mathbb{E}[dW_i] = 0$, for $i,j = X_l, P_l$, where $\mathbb{E}$ represents the stochastic average. The SME of Eq. (2) is valid provided the cavity can be adiabatically eliminated, which is readily achieved in the unresolved-sideband regime, and for resolved-sideband systems, κ must be larger than the interaction rate [49].

For a continuous-input drive, the measurement records of the X_l and P_l homodyne detectors are $dy_{X_l} = \langle f_R\rangle dt + dW_{X_l}/\sqrt{8\eta(1-\zeta^2)k}$ and $dy_{P_l} = \langle f_I\rangle dt + dW_{P_l}/\sqrt{8\eta\zeta^2 k}$, respectively [55,56]. And, the general-dyne measurement currents are defined by $X_l(t) = \sqrt{4k\eta(1-\zeta^2)/\tau}\int_{t-\tau}^{t} dy_{X_l}$ and $P_l(t) = \sqrt{4k\eta\zeta^2/\tau}\int_{t-\tau}^{t} dy_{P_l}$, where τ is the integration time of the homodyne detectors. Here, $1/\tau$ must be much faster than all other relevant rates, such that the SME in Eq. (2) accurately models the continuous measurement [57]. Also, at $\mu = 0$ the measurement currents are normalized to give $\mathbb{E}(X_l^2) - \mathbb{E}(X_l)^2 = \mathbb{E}(P_l^2) - \mathbb{E}(P_l)^2 = 1/2$, $\mathbb{E}(P_l) = 0$, and $\mathbb{E}(X_l) = X_\alpha\sqrt{\eta(1-\zeta^2)}$, with $X_\alpha^2 = 4k\tau$.

For small optical rotations ($\mu\sigma \ll 1$), Eq. (2) reduces to the standard SME of linearized optomechanics as $c = \sqrt{2k}f(X_m) \approx \sqrt{2k} + i\sqrt{2\mu^2 k}X_m$ and $\mu^2 k$ recovers the linearized measurement rate $2g^2/\kappa$, where g is the linearized coupling rate [58,59]. However, we find that a distinct Gaussian limit of Eq. (2) exists beyond linearized optomechanics for arbitrarily large optical rotations. Curiously, in this regime, the evolution of the mechanical covariance matrix is *stochastic* as the variances depend on the measurement outcomes. We thus term this new Gaussian regime of operation the *stochastic Gaussian regime*. To derive this regime, at every time step $t \to t + dt$ we write $\mu X_m = \mu\langle X_m\rangle + \mu Y_m$ in Eq. (2). Provided $\mathrm{Var}(\mu Y_m) \ll 1$, which implies weak single-photon coupling, we then expand the SME to first order in μY_m, and the small optical phase shifts μY_m may be integrated to obtain arbitrarily large optical rotations over a finite duration. Introducing $\mathbf{r} = (Y_m, P_m)^{\mathrm{T}}$, the dynamics of the first moments $\langle\mathbf{r}\rangle = \mathrm{tr}(\rho\mathbf{r})$ and the covariance matrix elements $V_{ij} = \langle\{r_i, r_j\}\rangle/2 - \langle r_i\rangle\langle r_j\rangle$ can be computed from the Gaussian approximation to Eq. (2). In the stochastic Gaussian regime, the dynamics of an initial Gaussian mechanical state are completely described by a stochastic differential equation for $\langle\mathbf{r}\rangle$ and a stochastic Riccati equation for V:

$$d\langle\mathbf{r}\rangle = (M\langle\mathbf{r}\rangle + \mathbf{d})dt + N\sqrt{\boldsymbol{\eta}}d\mathbf{W}, \quad (3)$$

$$\dot{V} = MV + VM^{\mathrm{T}} + D - N\boldsymbol{\eta}N^{\mathrm{T}}. \quad (4)$$

Here, $\boldsymbol{\eta} = \mathrm{diag}(\eta,\eta,0)$ and $d\mathbf{W} = (dW_{X_l}, dW_{P_l}, 0)^{\mathrm{T}}$. We have also introduced the displacement vector $\mathbf{d}$ and the drift M, diffusion D, and noise N matrices, given in the Supplemental Material [49]. See, e.g., Ref. [60] for other usage of the Riccati equation. Note, Eq. (4) is stochastic as M, D, and N depend on the mean position $\langle X_m\rangle$.

For a fixed drive frequency at $\Delta = 0$, the optical phase shift averaged over a given stochastic trajectory is positive because the radiation-pressure force causes a nonzero time-averaged mean mechanical position. Hence, to maximize the amount of light that enters the cavity, and ensure the time-averaged optical phase shift is zero, we model a lock of the pump field to the mean cavity resonance frequency using a third-order Butterworth filter with a cutoff frequency at $0.5\omega_m$. This locking effectively cancels the slowly varying component of $\langle X_m\rangle$, while the dynamics and fluctuations of the mechanical position are still measured.

The dynamics of the mechanical Gaussian state governed by Eqs. (3) and (4) are solved numerically using an Euler-Maruyama method [61]. Here, we use a parameter set (see the caption of Fig. 3) based on sliced-photonic crystal structures [17,45], and more parameter sets are explored in the Supplemental Material [49]. For this continuous measurement, we choose a beam splitter coefficient of $\zeta = 1/\sqrt{2}$ corresponding to heterodyne detection, which is readily implemented using a single balanced detector and a frequency-offset local oscillator. Figure 3(a) shows the general-dyne measurement currents with time for a given stochastic trajectory, and the corresponding means $\langle X_m\rangle$ and $\langle P_m\rangle$ are plotted in Fig. 3(b). We see the evolution of the means is anharmonic resulting from the optomechanical nonlinearities. Meanwhile, Fig. 3(c) plots the general-dyne currents as a 2D histogram in optical phase space, which is symmetric due to the drive locking. Figure 3(d) shows the position variance V_X, the momentum variance V_P, and the minimum eigenvalue of the covariance matrix V_{min} for

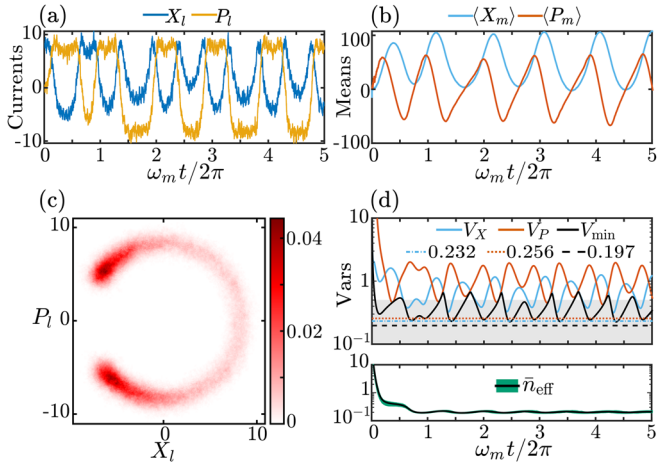

FIG. 3. Nonlinear continuous position measurement in the stochastic Gaussian regime. Here, $X_\alpha/\sqrt{2}=10$, $\omega_m/2\pi=10$ MHz, $\mu=0.05$, $\mu^2k/\omega_m=2$, $\eta=0.7$, $\gamma/2\pi=10$ Hz, $\zeta=1/\sqrt{2}$, $T=4$ K ($\bar{n}=8.4\times10^3$), and the initial mechanical state is precooled to 100 mK ($\bar{n}=2.1\times10^2$). (a) The general-dyne measurement currents X_l and P_l plotted as a function of time for a given trajectory. (b) The corresponding trajectories of the mechanical means $\langle X_m\rangle$ and $\langle P_m\rangle$. (c) The same general-dyne currents plotted as a normalized 2D histogram. (d) Top: the position variance V_X, the momentum variance V_P, and the minimum eigenvalue $V_{\min}$ for the same trajectory. Here, the dashed lines correspond to the mean of the minimum of each variance quantity over 100 trajectories and the gray shaded area indicates quantum squeezing. Bottom: the effective thermal occupation $\bar{n}_{\rm eff}$ averaged over 100 trajectories, where the shaded green area indicates the upper and lower quartile range.

the same trajectory, and the dashed lines indicate the mean of the minimum value of these quantities over 100 runs, each lasting 100 mechanical periods. We also plot the effective thermal occupation $\bar{n}_{\rm eff}=\sqrt{\det(V)}-1/2=[1/{\rm tr}(\rho^2)-1]/2$ averaged over the 100 runs. These plots show that for the modest parameters used here, quantum squeezing below 3 dB ($V_{\min},V_X<0.25$) and effective ground-state cooling are achievable in the stochastic Gaussian regime.

Conclusions and outlook.—We introduce a framework for cavity quantum optomechanics that captures the nonlinearities of both radiation pressure and the cavity response. As a natural first application of this framework, we study mechanical position measurement in the presence of these nonlinearities, which enables mechanical information encoded on both optical quadratures throughout the full cavity phase response of $\pm\pi$ to be measured via optical general-dyne detection. Our scheme can be employed with backaction-evading pulsed measurements or with continuous measurements, and we derive a measurement operator and a stochastic master equation for each mode of operation, respectively. As well as recovering the linearized theory, our framework is capable of describing the three regimes where the linearized approximation fails: (i) the weak single-photon-coupling regime but with significant optical rotations, (ii) the strong single-photon-coupling regime, and (iii) systems operating at low light levels. Thus, this treatment vastly extends the range that cavity optomechanical position measurement can be performed and enables the identification of new regimes of operation, such as the stochastic Gaussian regime we identify and term here. In addition to describing how to perform mechanical quantum squeezing by measurement in nonlinear systems, our formalism will also lead to a broad range of experimental and theoretical advances in sensing, mechanical quantum state engineering, and quantum measurement and control.

We acknowledge useful discussions with G. A. Brawley, R. Clarke, G. Enzian, L. A. Kanari-Naish, G. J. Milburn, B. A. Stickler, and S. Qvarfort. This project was supported by the Engineering and Physical Sciences Research Council (EP/T031271/1), UK Research and Innovation (MR/S032924/1), the Royal Society, and the European Research Council (ERC Starting Grant No. 759644-TOPP). This work is part of the research program of the Netherlands Organisation for Scientific Research (NWO) and supported by an NWO Vidi grant.

*jack.clarke@imperial.ac.uk
†m.vanner@imperial.ac.uk; www.qmeas.net.

[1] A. Kronwald and F. Marquardt, Phys. Rev. Lett. **111**, 133601 (2013).
[2] K. Børkje, A. Nunnenkamp, J. D. Teufel, and S. M. Girvin, Phys. Rev. Lett. **111**, 053603 (2013).
[3] M. A. Lemonde, N. Didier, and A. A. Clerk, Phys. Rev. Lett. **111**, 053602 (2013).
[4] M. R. Vanner, Phys. Rev. X **1**, 021011 (2011).
[5] S. Bose, K. Jacobs, and P. L. Knight, Phys. Rev. A **59**, 3204 (1999).
[6] M. Ringbauer, T. J. Weinhold, L. A. Howard, A. G. White, and M. R. Vanner, New J. Phys. **20**, 053042 (2018).
[7] J. Clarke and M. R. Vanner, Quantum Sci. Technol. **4**, 014003 (2019).
[8] W. Marshall, C. Simon, R. Penrose, and D. Bouwmeester, Phys. Rev. Lett. **91**, 130401 (2003).
[9] G. Vacanti, M. Paternostro, G. M. Palma, and V. Vedral, New J. Phys. **10**, 095014 (2008).
[10] U. Akram, W. P. Bowen, and G. J. Milburn, New J. Phys. **15**, 093007 (2013).
[11] L. A. Kanari-Naish, J. Clarke, S. Qvarfort, and M. R. Vanner, Quantum Sci. Technol. **7**, 035012 (2022).
[12] P. Rabl, Phys. Rev. Lett. **107**, 063601 (2011).
[13] A. Nunnenkamp, K. Børkje, and S. M. Girvin, Phys. Rev. Lett. **107**, 063602 (2011).
[14] F. Brennecke, S. Ritter, T. Donner, and T. Esslinger, Science **322**, 235 (2008).
[15] T. P. Purdy, D. W. C. Brooks, T. Botter, N. Brahms, Z.-Y. Ma, and D. M. Stamper-Kurn, Phys. Rev. Lett. **105**, 133602 (2010).

[16] G. A. Brawley, M. R. Vanner, P. E. Larsen, S. Schmid, A. Boisen, and W. P. Bowen, Nat. Commun. **7**, 10988 (2016).
[17] R. Leijssen, G. R. La Gala, L. Freisem, J. T. Muhonen, and E. Verhagen, Nat. Commun. **8**, 16024 (2017).
[18] S. A. Fedorov, A. Beccari, A. Arabmoheghi, D. J. Wilson, N. J. Engelsen, and T. J. Kippenberg, Optica **7**, 1609 (2020).
[19] A. G. Krause, M. Winger, T. D. Blasius, Q. Lin, and O. Painter, Nat. Photonics **6**, 768 (2012).
[20] F. Guzmán Cervantes, L. Kumanchik, J. Pratt, and J. M. Taylor, Appl. Phys. Lett. **104**, 221111 (2014).
[21] J. Chaste, A. Eichler, J. Moser, G. Ceballos, R. Rurali, and A. Bachtold, Nat. Nanotechnol. **7**, 301 (2012).
[22] G. Ranjit, M. Cunningham, K. Casey, and A. A. Geraci, Phys. Rev. A **93**, 053801 (2016).
[23] D. Rugar, R. Budakian, H. J. Mamin, and B. W. Chui, Nature (London) **430**, 329 (2004).
[24] G. Longo, L. Alonso-Sarduy, L. M. Rio, A. Bizzini, A. Trampuz, J. Notz, G. Dietler, and S. Kasas, Nat. Nanotechnol. **8**, 522 (2013).
[25] B. P. Abbott *et al.* (LIGO Scientific and Virgo Collaborations), Phys. Rev. Lett. **116**, 061102 (2016).
[26] D. C. Moore and A. A. Geraci, Quantum Sci. Technol. **6**, 014008 (2021).
[27] D. Carney, G. Krnjaic, D. C. Moore, C. A. Regal, G. Afek, S. Bhave, B. Brubaker, T. Corbitt, J. Cripe, N. Crisosto *et al.*, Quantum Sci. Technol. **6**, 024002 (2021).
[28] A. A. Geraci, S. J. Smullin, D. M. Weld, J. Chiaverini, and A. Kapitulnik, Phys. Rev. D **78**, 022002 (2008).
[29] V. B. Braginsky and F. Y. Khalili, *Quantum Measurement* (Cambridge University Press, Cambridge, England, 1995).
[30] K. W. Murch, K. L. Moore, S. Gupta, and D. M. Stamper-Kurn, Nat. Phys. **4**, 561 (2008).
[31] T. P. Purdy, R. W. Peterson, and C. A. Regal, Science **339**, 801 (2013).
[32] J. Cripe, N. Aggarwal, R. Lanza, A. Libson, R. Singh, P. Heu, D. Follman, G. D. Cole, N. Mavalvala, and T. Corbitt, Nature (London) **568**, 364 (2019).
[33] A. C. Doherty and K. Jacobs, Phys. Rev. A **60**, 2700 (1999).
[34] S. Mancini, D. Vitali, and P. Tombesi, Phys. Rev. Lett. **80**, 688 (1998).
[35] P. F. Cohadon, A. Heidmann, and M. Pinard, Phys. Rev. Lett. **83**, 3174 (1999).
[36] D. J. Wilson, V. Sudhir, N. Piro, R. Schilling, A. Ghadimi, and T. J. Kippenberg, Nature (London) **524**, 325 (2015).
[37] M. Rossi, D. Mason, J. Chen, Y. Tsaturyan, and A. Schliesser, Nature (London) **563**, 53 (2018).
[38] V. B. Braginsky, Y. I. Vorontsov, and K. S. Thorne, Science **209**, 547 (1980).
[39] A. A. Clerk, F. Marquardt, and K. Jacobs, New J. Phys. **10**, 095010 (2008).
[40] J. Suh, A. J. Weinstein, C. U. Lei, E. E. Wollman, S. K. Steinke, P. Meystre, A. A. Clerk, and K. C. Schwab, Science **344**, 1262 (2014).
[41] I. Shomroni, L. Qiu, D. Malz, A. Nunnenkamp, and T. J. Kippenberg, Nat. Commun. **10**, 2086 (2019).
[42] V. B. Braginsky, Y. I. Vorontsov, and F. Y. Khalili, JETP Lett. **27** (1978).
[43] M. R. Vanner, I. Pikovski, G. D. Cole, M. S. Kim, Č. Brukner, K. Hammerer, G. J. Milburn, and M. Aspelmeyer, Proc. Natl. Acad. Sci. U.S.A. **108**, 16182 (2011).
[44] M. R. Vanner, J. Hofer, G. D. Cole, and M. Aspelmeyer, Nat. Commun. **4**, 2295 (2013).
[45] J. T. Muhonen, G. R. La Gala, R. Leijssen, and E. Verhagen, Phys. Rev. Lett. **123**, 113601 (2019).
[46] N. Walker and J. E. Carroll, Opt. Quantum Electron. **18**, 355 (1986).
[47] A. Furusawa, J. L. Sørensen, S. L. Braunstein, C. A. Fuchs, H. J. Kimble, and E. S. Polzik, Science **282**, 706 (1998).
[48] M. D. Vidrighin, G. Donati, M. G. Genoni, X.-M. Jin, W. S. Kolthammer, M. S. Kim, A. Datta, M. Barbieri, and I. A. Walmsley, Nat. Commun. **5**, 3532 (2014).
[49] See Supplemental Material at http://link.aps.org/supplemental/10.1103/PhysRevLett.131.053601 for further theoretical details and an animation of the optical Husimi-*Q* function.
[50] I. Pikovski, M. R. Vanner, M. Aspelmeyer, M. S. Kim, and Č. Brukner, Nat. Phys. **8**, 393 (2012).
[51] Z. Wang and A. H. Safavi-Naeini, Nat. Commun. **8**, 15886 (2017).
[52] U. Leonhardt, *Measuring the Quantum State of Light* (Cambridge University Press, Cambridge, England, 1997), Vol. 22.
[53] Note that an outcome window may be utilized to further reduce the variance at the cost of introducing a finite window-dependent heralding probability.
[54] M. A. Schlosshauer, *Decoherence: And the Quantum-to-Classical Transition* (Springer Science & Business Media, New York, 2007).
[55] K. Jacobs and D. A. Steck, Contemp. Phys. **47**, 279 (2006); K. Jacobs, *Quantum Measurement Theory and Its Applications* (Cambridge University Press, Cambridge, England, 2014).
[56] H. M. Wiseman and G. J. Milburn, *Quantum Measurement and Control* (Cambridge University Press, Cambridge, England, 2009).
[57] C. M. Caves and G. J. Milburn, Phys. Rev. A **36**, 5543 (1987).
[58] M. Rossi, D. Mason, J. Chen, and A. Schliesser, Phys. Rev. Lett. **123**, 163601 (2019).
[59] C. Meng, G. A. Brawley, J. S. Bennett, M. R. Vanner, and W. P. Bowen, Phys. Rev. Lett. **125**, 043604 (2020).
[60] J. Zhang and K. Mølmer, Phys. Rev. A **96**, 062131 (2017).
[61] K. Jacobs, *Stochastic Processes for Physicists: Understanding Noisy Systems* (Cambridge University Press, Cambridge, England, 2010).